




Open Archive Toulouse Archive Ouverte (OATAO)

OATAO is an open access repository that collects the work of Toulouse researchers and makes it freely available over the web where possible

This is an author's version published in: <http://oatao.univ-toulouse.fr/21003>

Official URL: <https://doi.org/10.1016/j.molliq.2017.12.100>

To cite this version:

Kopac, Turkan and Bozgeyik, Kadriye and Flahaut, Emmanuel 
Adsorption and interactions of the bovine serum albumin-double walled carbon nanotube system. (2018) *Journal of Molecular Liquids*, 252. 1-8. ISSN 0167-7322

Any correspondence concerning this service should be sent to the repository administrator: tech-oatao@listes-diff.inp-toulouse.fr

Adsorption and interactions of the bovine serum albumin-double walled carbon nanotube system

Turkan Kopac^{a,*}, Kadriye Bozgeyik^a, Emmanuel Flahaut^b

^a Department of Chemistry, Bülent Ecevit University, 67100 Zonguldak, Turkey

^b CIRIMAT, Université de Toulouse, CNRS, INPT, UPS, UMR CNRS-UPS-INP N°5085, Université Toulouse 3 Paul Sabatier, Bât. CIRIMAT, 118, route de Narbonne, 31062 Toulouse cedex 9, France

ARTICLE INFO

Keywords:

Adsorption

Double walled carbon nanotubes

Bovine serum albumin

ABSTRACT

Adsorption and interactions of Bovine Serum Albumin (BSA) with Double Walled Carbon Nanotubes (DWNT) prepared by catalytic chemical vapor deposition (CCVD) synthesis were studied. Adsorption kinetics and equilibrium were investigated by means of in situ UV-spectroscopy. The extent of adsorption at different temperatures was determined at the end of a 420-min adsorption period. The adsorption equilibrium experiments were performed using various amounts of nanotubes at pH 4 and 40 °C, and the adsorption parameters were evaluated comparing the experimental data with models such as the Freundlich and Langmuir isotherms. The maximum protein adsorption capacity (Q_0) of DWNT was determined as 1221 mg·g⁻¹. The effect of temperature on the adsorption rate experiments was investigated for constant amount of adsorbent at pH 4. Adsorption kinetics followed the pseudo-first-order rate. Zeta potential measurements were performed with respect to solution pH for understanding the protein-surface interactions. The interactions between positively charged BSA molecules with negatively charged DWNT at pH 4 were found to be electrostatic attractions. Thermodynamic parameters, ΔH^0 and ΔS^0 were found as 9.40 kJ·mol⁻¹ and 321.5 J·mol⁻¹ K⁻¹, respectively. ΔH^0 value indicated that BSA adsorption on DWNT was a physisorption process.

1. Introduction

Adsorption of proteins on solid surfaces is important in natural sciences, medicine and industry, and has an important role in numerous applications such as protein chips, biosensors, food industry and medical implants [1,2]. In many applications related with biomedicine, as the interactions between proteins, implants and cells might have undesirable effects, inert surfaces should be used. For this reason, such kind of surfaces have been synthesized with various forms of surface modifications to inhibit the adsorption on the surfaces [3]. Also, there are applications where the surface adsorption and interactions are desired, in that case surface modifications are made in order to enhance the adsorption. In terms of potential toxicity and biodistribution in the body, it is well known that the corona of adsorbed proteins plays a determining role in the fate of nanoparticles [4], and particles in general. Following the discovery of carbon nanotubes (CNT) and because of their many potential uses including different biomedical applications, the interaction of biomolecules with CNT has been investigated in terms of biocompatibility, usefulness as platforms to support growth of nerve cells [5] or bioelectronic sensors [6]. CNTs having unique electronic, mechanical and structural properties are also exploited in the field of materials

science [7]. CNTs are in the form of tubular hexagonal carbon structures which are capped by half fullerene molecules. The main types of CNTs are single-walled (SWNT), double-walled (DWNT) and multi-walled (MWNT) carbon nanotubes [8]. DWNT are at the interface between SWNT and MWNT with >2 walls, they combine the morphology and flexibility of the former with the physico-chemical resistance of the latter and can thus be considered as a good mode of "carbon nanotubes" in general. The dimensions of their structures range in between 0.4–2 nm in diameter for SWNT and 2–100 nm for MWNT. Their length typically ranges from 1 to 50 μm. DWNTs have diameters typically ranging in between 1 and 3 nm and lengths from several to tens of micrometers [9]. DWNTs have a strong tendency to agglomerate and are practically not soluble in solvents because of their strong hydrophobicity and van der Waals interactions within bundles. However, for potential applications in the fields of biology and biomedicine, solubility in aqueous solution is important [10]. Chen et al. [11] noted that protein adsorption on SWNT field effect transistors led to appreciable changes in the electrical conductance of the devices that could be utilized for label-free detection of biomolecules. It was also reported that electronic effects occurring at the nanotube-metal interfaces due to protein adsorption constituted a more significant contribution to the electronic biosensing signal than adsorption solely along the lengths of CNTs. Salvador-Morales et al. [12] investigated the protein binding to purified CNTs in human plasma and serum. They reported that when MWNTs were exposed to the

* Corresponding author.

E-mail address: turkan.kopac@beun.edu.tr (T. Kopac).

human plasma and serum, only a few kinds of proteins were able to bind MWNTs. Roman et al. [13] investigated the amino acids adsorption on graphite sheets and CNTs through density functional theory. They reported weak binding of the biomolecules on both CNTs and graphite sheets, but generally favorable adsorption pathways were observed. Zwitterion adsorption through the charged carboxylate and amine groups were bound stronger to the CNT surface as compared to the non-ionic counterparts, phenylalanine, histidine, and cysteine side chain groups. Binding strengths on graphite did not show similar trends for amino acid interactions with the increase in CNT diameter. In order for CNTs to be used as biosensors or drug delivery carriers, information regarding whether protein or enzyme biomolecules could bind with CNT is rather important.

Adsorption of BSA to various surfaces such as gold nanoparticles, gold electrodes, polypyrrole-based adsorbents, neutral and charged hydrophilic and hydrophobic surfaces, silica, poly(hydroxyethylmethacrylate)-Reactive Green 19 cryogel disks, mica, polymeric nanoparticles, chromium(III) oxide suspension, zirconia nanoparticles were investigated in some of the reported literature studies [14–23]. In recent years, there are only a few studies related with the investigation of the adsorption and the attractions between the proteins and carbon based nanomaterials [5,21–29].

In our previous works, the kinetics and equilibrium of BSA adsorption onto several metal oxides (TiO_2 , Al_2O_3 , ZnO_2) and attraction interactions of surface-protein by zeta potential measurements were investigated [30–32]. The adsorption of BSA on MWNTs and SWNTs were also carried out and compared with the results of metal oxide adsorption studies [33,34]. The optimum conditions for protein adsorption on metal oxides and CNTs were found as pH 4 and 40 °C. In the present study, we focused on the equilibrium and kinetics of adsorption behavior of BSA on clean DWNTs prepared by a catalytic chemical vapor deposition (CCVD) synthesis that involved the use of a MgO-based catalyst [9]. The equilibrium and kinetics of BSA on DWNTs were examined at optimum solution conditions (pH: 4, T: 40 °C) determined in the previous studies [30–34]. The electrokinetic properties of protein adsorption were also examined to determine the interactions between BSA with DWNTs. The protein capacity of DWNTs, at same experimental conditions, was compared with protein capacities of metal oxides and other carbon nanotubes.

2. Experimental

DWNTs used in this work were prepared by CCVD synthesis using a MgO-based catalyst containing Co and Mo as the active elements. The details of the synthesis and sample processing were described earlier [9]. Clean CNTs, obtained in gram-scale amounts, contained ca. 80% DWNTs, the rest of the CNTs corresponding to ca. 5% of SWNT and 15% of triple-walled CNTs [9]. Pore characterization and specific surface

area of DWNT sample were done using a Quantachrome Automated Gas Sorption Analyzer. Brunauer-Emmett-Teller (BET), Barrett-Joyner-Halenda (BJH) and non-local density functional theory (NLDFT) techniques were used for the surface area, pore size and pore volume analysis of the sample. TGA, operated in air atmosphere at 1°/min, was performed using a SETARAM TAG24 thermobalance. The morphology was observed by transmission electron microscopy (JOEL 2100F) with a maximum acceleration of 100 kV. Raman spectroscopy was performed using a Jobin Yvon LABRAM spectrometer (green laser at 532 nm) with a maximum power of 2 mW.

The effects of working parameters such as adsorbent dosage ($0.2\text{--}1.0\text{ g}\cdot\text{L}^{-1}$) and temperature (25, 30, 37, 40 °C) on BSA adsorption were studied in a batch adsorber for a specific period of contact time. Merck grade BSA (12,657, fraction V) was used as received. The BSA solutions were prepared in 0.15 M NaCl solution at $0.60\text{ g}\cdot\text{L}^{-1}$. Adjustment of solution pH was done using a $\text{NaH}_2\text{PO}_4\cdot 2\text{H}_2\text{O}/\text{H}_3\text{PO}_4$ buffer solution (pH 2.8). For equilibrium and kinetic studies, 100 mL of protein solution at constant initial concentration and at constant pH 4 was taken in a 250 mL flask and agitated in a shaking water bath for 420 min contact time at 100 rpm speed. Equilibrium experiments were conducted with different concentrations of DWNT as adsorbent ($0.2\text{--}1.0\text{ g}\cdot\text{L}^{-1}$) at constant temperature (40 °C). Kinetic experiments were conducted at 25, 30, 37, 40 °C with a constant dose of adsorbent ($0.60\text{ g}\cdot\text{L}^{-1}$). At various time intervals, the solution sample was filtered and then analyzed using the method of Lowry [35] by a Shimadzu 1700-E spectrometer at a wavelength of 720 nm. The BSA concentration of the adsorbent phase (q_e , $\text{mg}\cdot\text{g}^{-1}$) was determined using,

$$q_e = \frac{(C_0 - C)V}{w} \quad (1)$$

where C_0 is the initial value of BSA concentrations ($\text{mg}\cdot\text{L}^{-1}$), C is the BSA concentration ($\text{mg}\cdot\text{L}^{-1}$) at any time, V denotes the volume (L) and w is the amount of DWNT (g). Some of the experiments were repeated in order to check the reproducibility of the measurements, and the relative errors obtained for the selected runs were found not to be higher than 3%.

Zeta potentials for DWNT were measured at a concentration of 0.02 wt% in $0.6\text{ mg}\cdot\text{mL}^{-1}$ BSA solution using a ZetaPlus zeta potential analyzer (Brookhaven Instruments Corporation) by electrophoresis light scattering method. All BSA solutions were prepared using $0.15\text{ mol}\cdot\text{L}^{-1}$ NaCl solution in order to keep the ionic strength constant, and the adjustment of the pH of the suspension was done using $\text{NH}_4\text{Cl}/\text{NH}_3$ and $\text{NaH}_2\text{PO}_4\cdot 2\text{H}_2\text{O}/\text{H}_3\text{PO}_4$ buffers, having pH 10 and 2.8, respectively. The electrophoretic mobility (μ_e) is related to the zeta potential (ζ) as shown by the following Hückel equation:

$$\mu_e = \frac{2e\zeta}{3\eta} \quad (2)$$

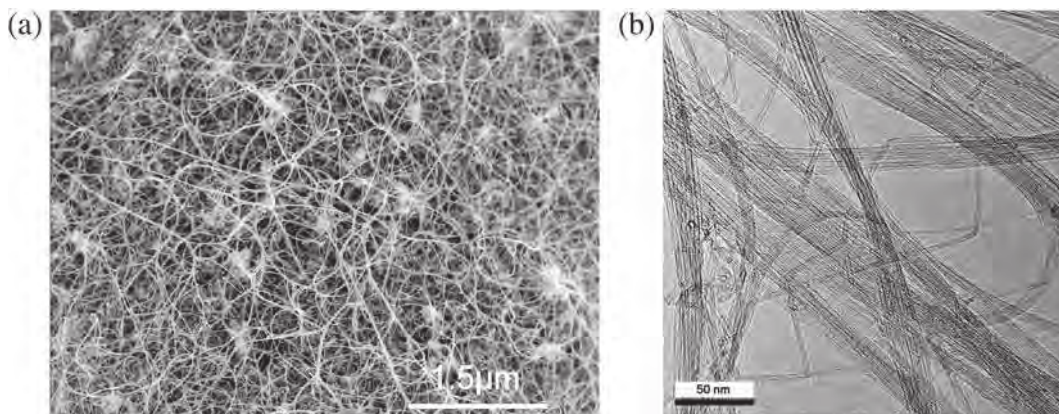


Fig. 1. Representative (a). SEM image (b). TEM image of DWNTs.

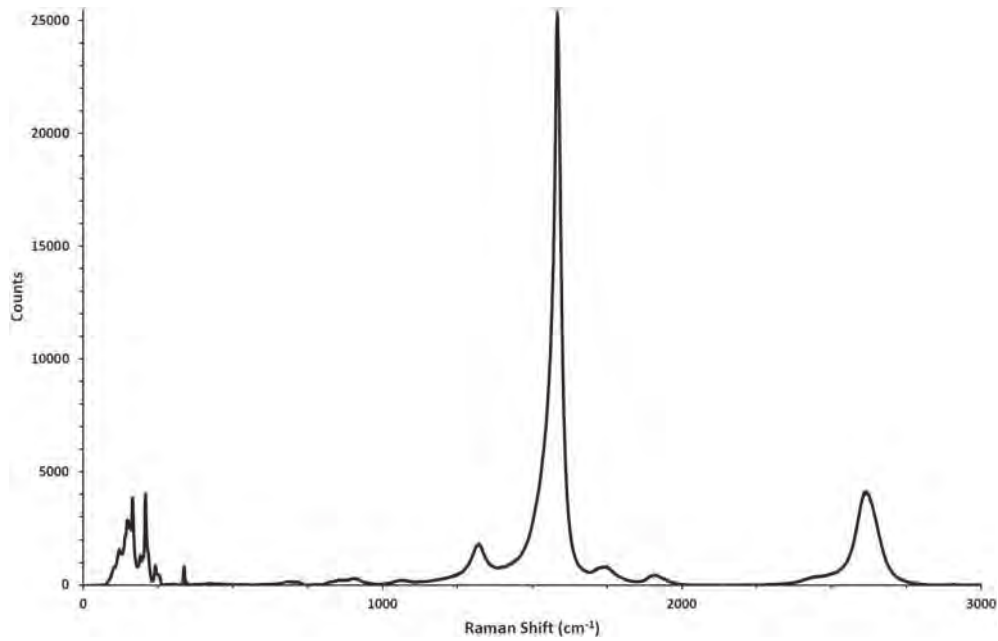


Fig. 2. Representative Raman spectrum of DWNTs (532 nm).

where η is the viscosity of the suspending liquid, and e is the dielectric constant.

3. Results and discussion

3.1. Characterization of DWNT

Characterization of the physical and chemical properties of DWNT is necessary to correlate the structure of DWNT with the adsorption behavior of protein. Fig. 1(a), (b) shows representative SEM and TEM images of the DWNT samples, revealing the simultaneous presence of sections with individual nanotubes, but mainly a bundle organization. Raman spectroscopy (Fig. 2) reveals a low level of defects with a very low ratio of intensity between the D and G bands ($I_D / I_G = 7\%$) [36] as well as carbon nanotubes with a diameter range between 1 and 2 nm (for those visible at 532 nm). The thermogravimetric analysis consists in heating the sample in air and monitoring the weight variation versus temperature. At a temperature close to 330 °C (as indicated by the derivative curve - in red), the combustion of CNTs in air starts to induce some weight loss (combustion of the CNTs in air). Simultaneously, the oxidation of the small amount of residual Co present in the sample leads to a very small weight gain (not visible on Fig. 3), due to Co

→ Co_3O_4 . This combustion of the CNTs is then almost completed at 600 °C, when the derivative curve becomes flat. The small weight loss at 932 °C corresponds to the final transformation of Co_3O_4 into CoO,

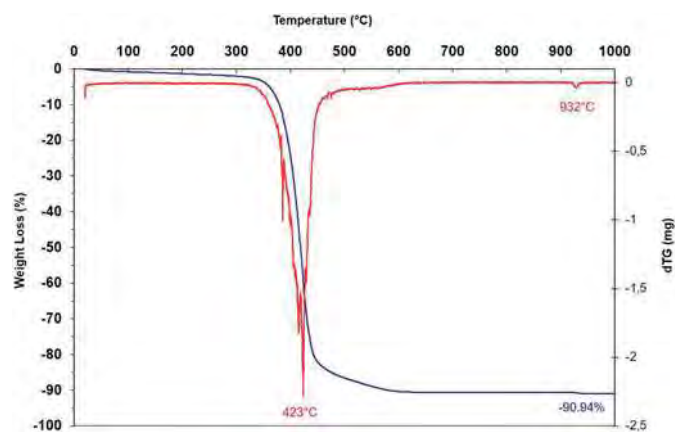


Fig. 3. TGA of DWNTs in air at 1 °C/min.

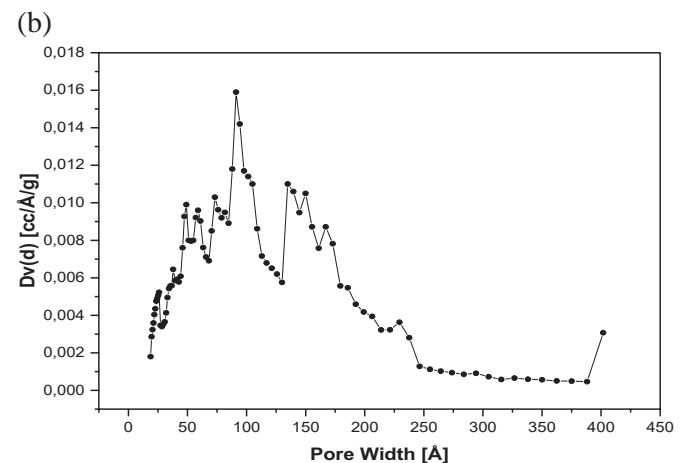
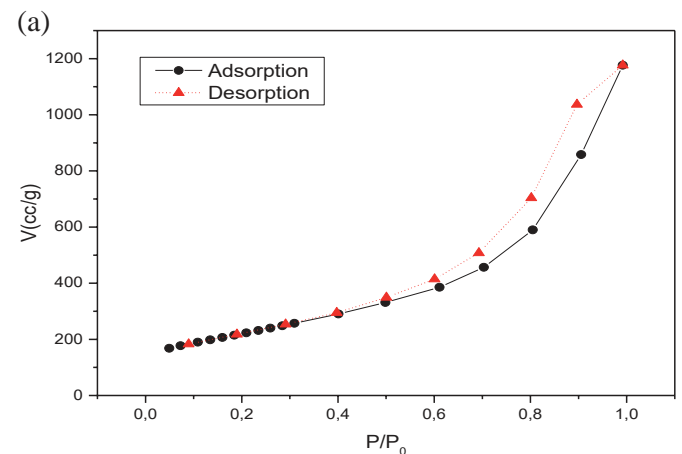


Fig. 4. (a) Adsorption-desorption isotherms of N_2 on DWNT (b) pore size distributions of DWNT.

Table 1
Surface area, pore size and pore volume of DWNT.

	BJH	NLDFT
Surface area, $\text{m}^2 \cdot \text{g}^{-1}$	771	780
Pore diameter, Å	24.36	91.14
Pore volume, $\text{cm}^3 \cdot \text{g}^{-1}$	1.794	1.729
BET surface area, $\text{m}^2 \cdot \text{g}^{-1}$	790.5	
Total pore volume ($P/P_0 = 0.995$), $\text{cm}^3 \cdot \text{g}^{-1}$	1.82	

and can be used to quantify the amount of residual Co present in the sample. From TGA analysis (Fig. 3) the concentration of residual metals can be estimated to 1.2 wt%. Adsorption-desorption isotherms of N_2 and pore size distributions of DWNT are shown in Fig. 4(a) and (b), respectively. Table 1 shows the surface properties of DWNT evaluated using the data shown in Fig. 4. According to the International Union of Pure and Applied Chemistry (IUPAC) classification, the pores may be divided in broad terms according to diameter (d) into macropores ($d > 50$ nm), mesopores ($2 < d < 50$ nm) and micropores ($d < 2$ nm) [37–38]. As demonstrated in Table 1 and Fig. 4(b), DWNT correspond to a mesoporous structure. The specific surface area found was $790.5 \text{ m}^2 \cdot \text{g}^{-1}$.

3.2. Zeta potential results

The main driving force for enzyme-solid interactions is an electrostatic force [39]. In order to understand the behavior of interactions, information about the electrostatic properties of BSA and DWNT are needed. Zeta potential measurements were performed for this purpose. Fig. 5 shows the changes in the zeta potentials of the DWNT, BSA and BSA-DWNT particles with respect to pH. The isoelectric point (pI) of BSA was determined as 4.7 in our previous studies, and the zeta potential values of BSA were positive below pI and negative above pI [33,34]. As shown from the figure, the DWNT particles were negatively charged at all pH levels, however BSA was positively charged at pH 4 only. The zeta potentials for the DWNT solution decreased (in absolute value) upon the addition of BSA, which can be attributed to the interfacial film formed due to the increase in the distance between the shear and the particle surfaces [40]. The decrease was higher for attraction interactions between BSA with DWNT particles at pH 4. This result shows that the maximum BSA adsorption onto DWNT particles occurs at pH 4.

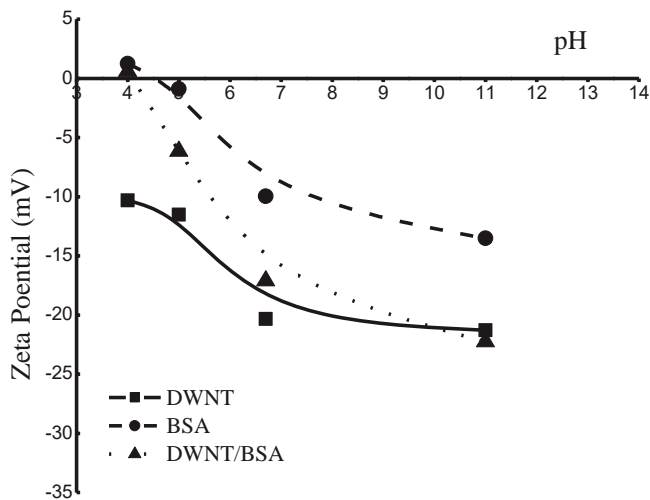


Fig. 5. Zeta potential curves for BSA adsorption on DWNT at different pH ($w: 5 \text{ g} \cdot \text{L}^{-1}$; $T: 20^\circ \text{C}$).

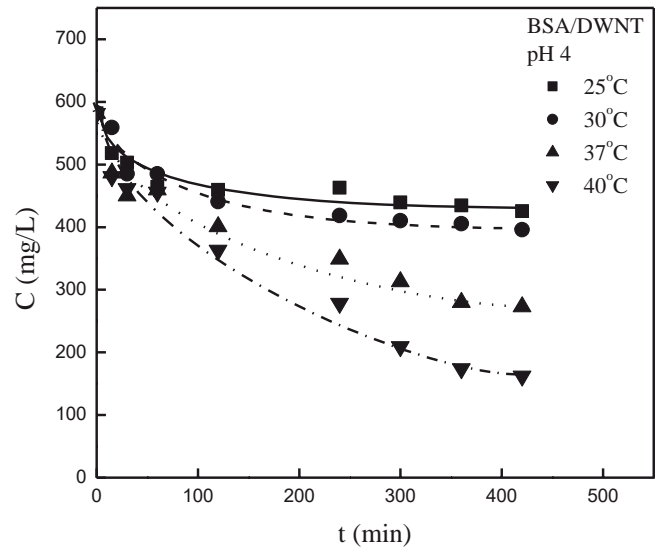


Fig. 6. Change of BSA solution concentration with time for adsorption on DWNT at different temperatures ($C_0: 581.5\text{--}582.6 \text{ mg} \cdot \text{L}^{-1}$; $\text{pH}: 4$; $w: 0.6 \text{ g} \cdot \text{L}^{-1}$; $V: 0.1 \text{ L}$).

3.3. Temperature effects

Fig. 6 shows the effect of solution temperature on BSA adsorption onto DWNT at constant initial concentration ($600 \text{ mg} \cdot \text{L}^{-1}$) and DWNT dosage ($0.6 \text{ g} \cdot \text{L}^{-1}$). From this figure, it was obvious that BSA adsorption onto DWNT at pH 4 was increased with increasing temperature. The BSA adsorption onto DWNT was higher at 40°C . For this study, the optimum experimental conditions were observed to be at pH 4 and 40°C . In our earlier studies, the optimum experimental condition for the maximum BSA adsorption onto the TiO_2 and the surface area enhanced TiO_2 were also found at pH 4 and 40°C [30].

3.4. Equilibrium analysis

Adsorption isotherm data are necessary for the design of adsorbers, and provide information about the adsorption capacity and the distribution of adsorption molecules between solid and liquid phases at equilibrium. The equilibrium isotherms were obtained by plotting BSA

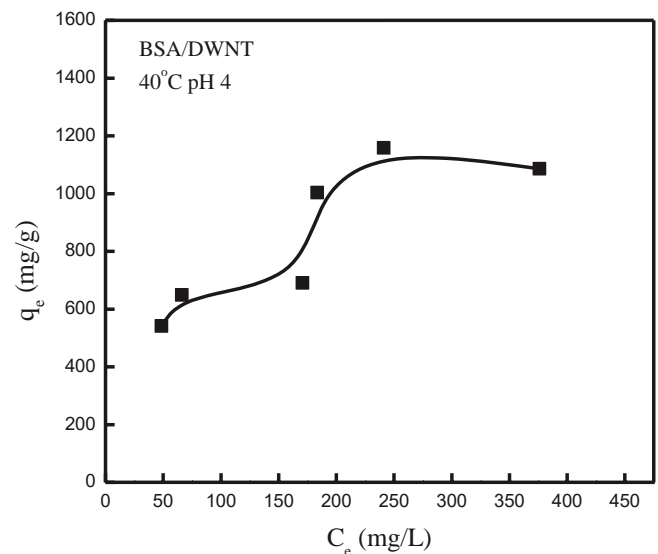


Fig. 7. q_e - C_e curve for BSA adsorption on DWNT ($\text{pH}: 4$; $w: 0.2\text{--}1 \text{ g} \cdot \text{L}^{-1}$; $V: 0.1 \text{ L}$).

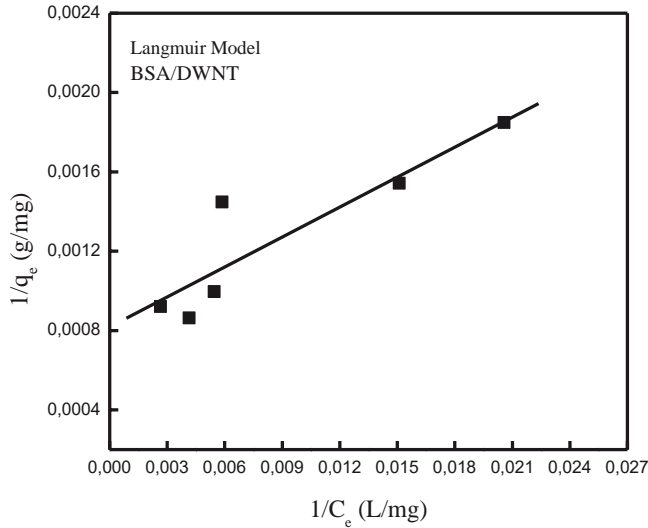


Fig. 8. Langmuir isotherm model curve for adsorption of BSA on DWNT (pH: 4; T: 40 °C; w: 0.2–1 g·L⁻¹).

adsorbed (q_e) against the BSA concentration left in solution (C_e) at equilibrium for various adsorbent dosages at pH 4 and 40 °C (Fig. 7).

The most frequently employed models, the Langmuir and the Freundlich equations, were used to express the equilibrium relationship during adsorption. The experimental equilibrium data at constant temperature and pH were compared with the model equations. The applicability of the isotherms for describing the process was judged by the values of the square of the correlation coefficient, r^2 . The Langmuir's isotherm [41] model is given below:

$$\frac{1}{q_e} = \frac{1}{Q_0} + \frac{1}{Q_0 b} \frac{1}{C_e} \quad (3)$$

where Q_0 and b are the constants related to adsorption capacity and the affinity of the binding sites, respectively. Plotting $1/q_e$ versus $1/C_e$ for the Langmuir isotherm, a straight line with a slope of $1/Q_0$ was obtained (Fig. 8). From the figure, the adsorption capacity of DWNT was found as 1221 mg·g⁻¹. Table 2 shows the model constants evaluated.

The linearized form of the Freundlich model is [42],

$$\log q_e = \log K_f + \left(\frac{1}{n}\right) \log C_e \quad (4)$$

where K_f and n are model constants. $1/n$ gives an indication of how favorable the adsorption process is, and K_f is the adsorption or distribution coefficient representing the amount of BSA adsorbed by DWNT at equilibrium. The slope ($1/n$) of the linearized equation ranging between 0 and 1 indicates the adsorption intensity or surface heterogeneity. As $1/n$ approaches to zero, the adsorbent surface gets more heterogeneous. $1/n < 1$ indicates a normal Langmuir isotherm, while $1/n > 1$ shows cooperative adsorption. The plot of $\log q_e$ against $\log C_e$ gave a straight line, and K_f was evaluated from the intercept (Fig. 9). The constants of K_f and $1/n$ together with r^2 values are also listed in Table 2. $1/n$ was found as 0.360, indicating a favorable adsorption. From the values of r^2 given in

Table 2
Langmuir and Freundlich model parameters for BSA adsorption onto DWNT at pH 4.

Temperature	Langmuir			Freundlich		
	Q_0 (mg·g ⁻¹)	b	r^2	K_f	$1/n$	r^2
40 °C	1221	0.00163	0.81	137.0	0.360	0.79

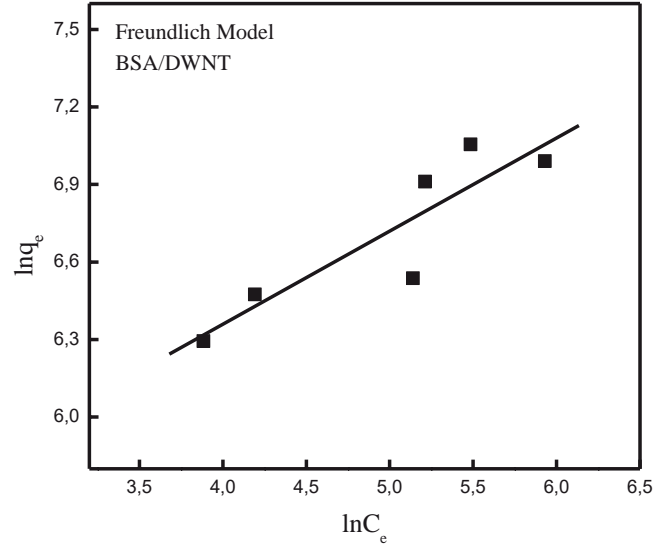


Fig. 9. Freundlich isotherm model curve for adsorption of BSA on DWNT (pH: 4; T: 40 °C; w: 0.2–1 g·L⁻¹).

Table 2, it can be seen that the adsorption data gave a better fit with the Langmuir equation than the Freundlich model.

The comparison of the BSA adsorption capacities of different adsorbents reported in our previously published articles [30–31], are also listed in Table 3. The DWNT samples used in this work exhibited the largest BSA adsorption capacity of 1221 mg·g⁻¹, when compared to our previously reported data regarding other kinds of CNTs.

3.5. Kinetic analysis

In order to investigate the temperature effects on the adsorption kinetic, the temperature was varied from 25 °C to 40 °C, while the initial BSA concentration held constant at 600 mg·L⁻¹ at the adsorbent dosage of 0.6 g·L⁻¹ (Fig. 6). The BSA adsorption efficiency values were found as 27%, 32%, 53% and 72% for the solution temperatures 25, 30, 37 and 40 °C, respectively. This showed that the adsorbate onto DWNT increased with increasing temperature at pH 4, which can be attributed to the availability of more adsorption sites and an increase in the sorptive surface area.

In order to search the rate controlling mechanism of BSA adsorption on DWNT samples, the pseudo-first-order and the pseudo-second-order equations were applied. The integrated equation of the pseudo-first-order rate [43] is given below,

$$\log(q_e - q) = \log q_e - \frac{k_1 t}{2.303} \quad (5)$$

where q (mg·g⁻¹) is the amount of BSA adsorbed on DWNT at time t , and k_1 (min⁻¹) is the rate constant.

Table 3
Comparison of maximum BSA adsorption capacity onto different adsorbents at pH 4 and 40 °C.

Adsorbents	Maximum BSA adsorption capacity (mg·g ⁻¹)	Reference
TiO ₂	42.6	Kopac et al. [27]
MWNT	139.5	Bozgeyik and Kopac [31]
SWNT	609.8	Kopac and Bozgeyik [30]
DWNT	1221	This work

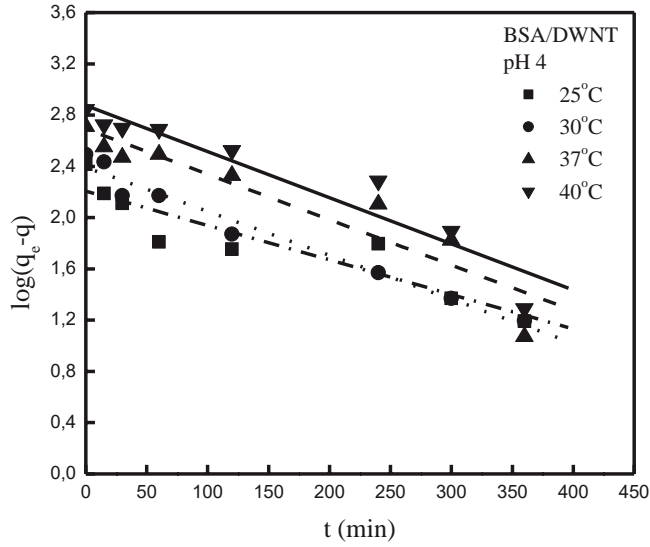


Fig. 10. Pseudo-first order rate curves obtained from adsorption of BSA on DWNT at different temperatures (C_0 : 581.5–582.6 mg·L⁻¹; pH: 4; w: 0.6 g·L⁻¹; V: 0.1 L).

An expression of the pseudo-second-order rate equation is given as [44],

$$\frac{1}{(q_e - q)} = \frac{1}{q_e} + k_2 t \quad (6)$$

where k_2 is the pseudo-second-order rate constant.

The slopes and intercepts of plots of $\log(q_e - q)$ versus t were obtained to determine the first-order rate constant k_1 (Fig. 10). r^2 values for the first-order model at pH 4 for 0.6 g·L⁻¹ of adsorbent dose were found as 0.85, 0.98, 0.88 and 0.90 for 25, 30, 37 and 40 °C, respectively. The evaluated parameters are all detailed in Table 4.

The slopes and the intercepts of plots of $1/(q_e - q)$ versus t were obtained to evaluate the rate constant k_2 (Fig. 11). In Table 4, values of k_2 and r^2 with respect to temperature are also presented. The r^2 values for the model at pH 4 for 0.6 g·L⁻¹ of DWNT amount are 0.82, 0.93, 0.54 and 0.59 for 25, 30, 37 and 40 °C, respectively. From the results it can be concluded that the pseudo first-order model was a better representative of the BSA adsorption onto DWNT. Further concerning rate constants, it was observed that k_1 values increased with an increase in temperature. This shows a change in the adsorption mechanism with an increase in temperature.

3.6. Thermodynamic analysis

Based on the basic concepts of the 1st and the 2nd laws of thermodynamics, energy of the system can neither be created nor destroyed and the only driving force is the entropy change. In order to gain insight into the adsorption mechanism, parameters such as changes in standard Gibbs free energy (ΔG^0), enthalpy (ΔH^0) and entropy (ΔS^0) were

Table 4
The values of k_1 and k_2 for BSA adsorption onto DWNT at pH 4 (w: 0.6 g·L⁻¹).

Temperature (°C)	pH 4			
	k_1 (min ⁻¹)	r^2	k_2 (g·mg ⁻¹ ·min ⁻¹)	r^2
25	0.0062	0.85	0.00014	0.82
30	0.0079	0.98	0.00016	0.93
37	0.0082	0.88	0.00015	0.54
40	0.0083	0.90	0.000093	0.59

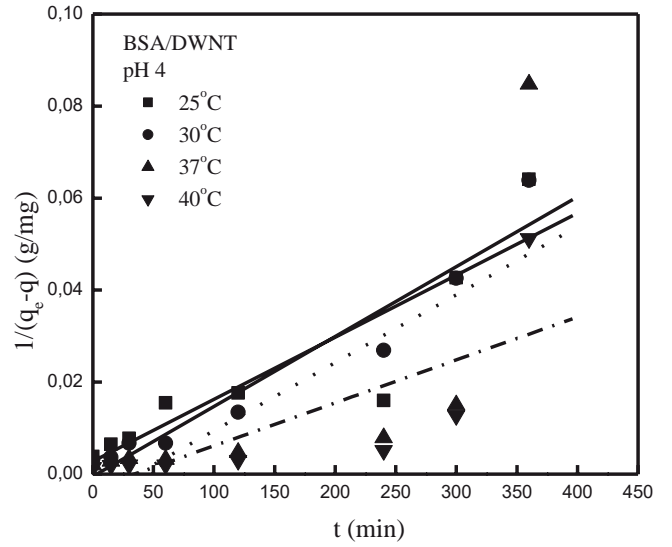


Fig. 11. Pseudo-second order rate curves obtained from adsorption of BSA on DWNT at different temperatures (C_0 : 581.5–582.6 mg·L⁻¹; pH: 4; w: 0.6 g·L⁻¹; V: 0.1 L).

evaluated from the plots of $\ln K_C$ versus $1/T$ (Fig. 12) considering Eqs. (6)–(8) [45].

$$K_C = \frac{q_e}{C_e} \quad (7)$$

$$\Delta G^0 = -RT \ln K_C \quad (8)$$

$$\ln K_C = \frac{\Delta S^0}{R} - \frac{\Delta H^0}{RT} \quad (9)$$

where K_C and R are the equilibrium and ideal gas constants.

The thermodynamic parameters calculated are presented in Table 5. ΔG^0 values estimated for adsorption of BSA onto DWNT were 1.22, 0.61, -1.64 and -3.80 kJ·mol⁻¹, respectively, at 298, 303, 310, and 313 K, indicating a spontaneous physisorption process [46]. As temperature increased from 298 to 310 K, ΔG^0 values decreased to negative values,

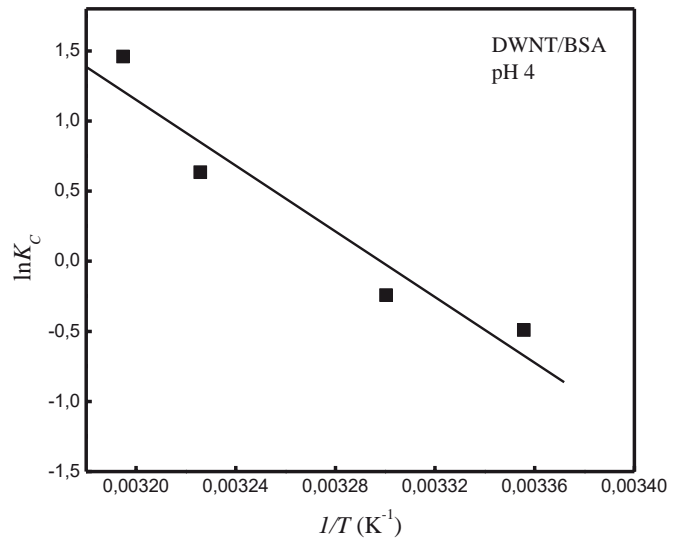


Fig. 12. The thermodynamic curve for BSA adsorption onto DWNT (pH: 4; w: 0.6 g·L⁻¹; V: 0.1 L).

Table 5

Values of thermodynamic parameters for the adsorption of BSA onto DWNT at pH 4 (w: 0.6 g·L⁻¹).

T (K)	ΔG (kJ·mol ⁻¹)	ΔH (kJ·mol ⁻¹)	ΔS (J·mol ⁻¹ ·K ⁻¹)
298	1.22	9.40	321.5
303	0.61		
310	-1.64		
313	-3.80		

suggesting that the adsorption was spontaneous at higher temperatures. ΔH^0 and ΔS^0 values of the process were 9.40 kJ·mol⁻¹ and 321.5 J·mol⁻¹ K⁻¹, respectively. The positive value for ΔH^0 indicates that the adsorption of BSA onto DWNT is an endothermic process. The magnitude of ΔH^0 is useful to a certain extent, in the classification of chemisorption and physisorption. Bonding strengths of <84 kJ·mol⁻¹ are typically considered as those of physisorption bonds [47]. Therefore, the value of ΔH^0 indicated that adsorption of BSA by DWNT was driven by a physisorption process. The positive value of ΔS^0 change reflects the affinity of the DWNT for BSA.

4. Conclusions

Adsorption of BSA by DWNT prepared by catalytic chemical vapor deposition (CCVD) synthesis was studied. The BSA adsorption isotherms gave a better fit with the Langmuir model. The maximum protein adsorption capacity (Q_0) was found as 1221 mg·g⁻¹ for DWNT. The effect of temperature onto adsorption rate experiments was investigated for constant amount of adsorbent at pH 4. Adsorption kinetics followed the pseudo-first-order rate, and k_1 values increased with an increase in temperature. Zeta potential measurements at different pH values were performed to understand the protein-surface interactions. The interactions between positively charged BSA molecules with negatively charged DWNT at pH 4 were found to be electrostatic attractions. The maximum BSA adsorption onto DWNT was at pH 4. The positive value for ΔH^0 (9.40 kJ·mol⁻¹) indicates that the adsorption of BSA onto DWNT is an endothermic process, and driven by a physisorption process.

References

- V.P. Zhdanov, B. Kasemo, Protein adsorption and desorption on lipid bilayers, *Biophys. Chem.* 146 (2010) 60–64.
- K. Szewczuk-Karpisz, M. Wiśniewska, Impact of lysozyme on stability mechanism of nanozirconia aqueous suspension, *Appl. Surf. Sci.* 379 (2016) 8–13.
- J.R. Wendorf, C.J. Radke, H.W. Blanch, The role electrolytes of protein adsorption at a hydrophilic solid-water interface, *Colloids Surf. B: Biointerfaces* 75 (2010) 100–106.
- A.E. Nel, L. Mädler, D. Velegol, T. Xia, E.M.V.P. Hoek, P. Somasundaran, F. Klaessig, V. Castranova, M. Thompson, Understanding biophysicochemical interactions at the nano-bio interface, *Nat. Mater.* 8 (2009) 543–557.
- A. Béduer, F. Seichepine, E. Flahaut, I. Loubinoux, L. Vaysse, C. Vieu, Elucidation of the role of carbon nanotube patterns on the development of cultured neuronal cells, *Langmuir* 28 (50) (2012) 17363–17371.
- J.N. Barisci, M. Tahhan, G.G. Wallace, S. Badaire, T. Vaugien, M. Maugey, P. Poulin, Properties of carbon nanotubes fibers spun from DNA-stabilized dispersions, *Adv. Funct. Mater.* 14 (2004) 133–138.
- R.C. Haddon, Special issue on carbon nanotubes, *Acc. Chem. Res.* 35 (2002) 997–1113.
- P.M. Ajayan, J.M. Lambert, P. Bernier, L. Barbedette, C. Colliex, J.M. Planeix, Growth morphologies during cobalt-catalyzed single-shell carbon nanotube synthesis, *Chem. Phys. Lett.* 215 (1993) 509–517.
- E. Flahaut, R. Bacsa, A. Peigney, C. Laurent, Gram-scale CCVD synthesis of double-walled carbon nanotubes, *Chem. Commun.* (2003) 1442–1443.
- E. Heister, C. Lamprecht, V. Neves, C. Tilmaciu, L. Datas, E. Flahaut, B. Soula, P. Hinterdorfer, H.M. Coley, S.R. Silva, J. McFadden, Higher dispersion efficacy of functionalized carbon nanotubes in chemical and biological environments, *ACS Nano* 4 (5) (2010) 2615–2626.
- R.J. Chen, H.C. Choi, S. Bangsaruntip, E. Yenilmez, X. Tang, Q. Wang, Y.L. Chang, H. Dai, An investigation of the mechanisms of electronic sensing of protein adsorption on carbon nanotube devices, *J. Am. Chem. Soc.* 126 (5) (2004) 1563–1568.
- C. Salvador-Morales, E. Flahaut, E. Simc, J. Sloan, M.L.H. Green, R.B. Simd, Complement activation and protein adsorption by carbon nanotubes, *Mol. Immunol.* 43 (2006) 193–201.
- T. Roman, W.A. Dino, H. Nakanishi, H. Kasai, Amino acid adsorption on single-walled carbon nanotubes, *Eur. Phys. J. D* 38 (2006) 117–120.
- M. Losin, V. Canpean, S. Astilean, Spectroscopic studies on pH- and thermally induced conformational changes of bovine serum albumin adsorbed onto gold nanoparticles, *J. Photochem. Photobiol. A Chem.* 217 (2–3) (2011) 395–401.
- X. Zhang, R. Bai, Y.W. Tong, Selective adsorption behaviors of proteins on polypyrrole-based adsorbents, *Sep. Purif. Technol.* 52 (1) (2006) 161–169.
- B. Beykal, M. Herzberg, Y. Oren, M.S. Mauter, Influence of surface charge on the rate, extent, and structure of adsorbed bovine serum albumin to gold electrodes, *J. Colloid Interface Sci.* 460 (2015) 321–328.
- H.T.M. Phan, S. Bartelt-Hunt, K.B. Rodenhausen, M. Schubert, J.C. Bartz, Investigation of bovine serum albumin (BSA) attachment onto self-assembled monolayers (SAMs) using combinatorial quartz crystal microbalance with dissipation (QCM-D) and spectroscopic ellipsometry (SE), *PLoS One* 10 (10) (2015), e0141282. <https://doi.org/10.1371/journal.pone.0141282>.
- M. Wiśniewska, K. Szewczuk-Karpisz, D. Sternik, Adsorption and thermal properties of the bovine serum albumin-silicon dioxide system, *J. Therm. Anal. Calorim.* 120 (2015) 1355–1364.
- N. Tuzmen, T. Kalburcu, D.A. Uygun, S. Akgol, A. Denizli, A novel affinity disks for bovine serum albumin purification, *Appl. Biochem. Biotechnol.* 175 (1) (2015) 454–468.
- B. Jachimska, A. Pajor, Physico-chemical characterization of bovine serum albumin in solution and as deposited on surfaces, *Bioelectrochemistry* 87 (2012) 138–146.
- J. Li, N.H. Wu, J.L. Wu, Y. Wan, C. Liu, Effect of protein adsorption on cell uptake and blood clearance of methoxy poly(ethylene glycol)-poly(caprolactone) nanoparticles, *J. Appl. Polym. Sci.* 133 (3) (2016) 42884, <https://doi.org/10.1002/app.42884>.
- K. Szewczuk-Karpisz, M. Wiśniewska, Investigation of removal possibilities of chromium(III) oxide from water solution in the presence of albumins, *Int. J. Environ. Sci. Technol.* 12 (2015) 2947–2956.
- K. Szewczuk-Karpisz, M. Wiśniewska, D. Myśliwiec, Albumin adsorption influence on the stability of the mesoporous zirconia suspension, *J. Ind. Eng. Chem.* 32 (2015) 113–119.
- J. Kuchlyan, N. Kundu, D. Banik, A. Roy, N. Sarkar, Spectroscopy and fluorescence lifetime imaging microscopy to probe the interaction of bovine serum albumin with graphene oxide, *Langmuir* 31 (51) (2015) 13793–13801.
- M. Sopotnik, A. Leonardi, I. Krizaj, P. Dusak, D. Makovec, T. Mesaric, N.P. Ulrih, I. Junkar, K. Sepcic, D. Drobne, Comparative study of serum protein binding to three different carbon-based nanomaterials, *Carbon* 95 (2015) 560–572.
- R.M.F. Fernandes, M. Buzaglo, O. Regev, E.F. Marques, I. Furo, Surface coverage and competitive adsorption on carbon nanotubes, *J. Phys. Chem. C* 119 (38) (2015) 22190–22197.
- G. Sekar, S. Vijayakumar, S. Thanigaivel, J. Thomas, A. Mukherjee, N. Chandrasekaran, Multiple spectroscopic studies on the interaction of BSA with pristine CNTs and their toxicity against *Donax faba*, *J. Lumin.* 170 (2016) 141–149.
- V.M.P. Barbosa, A.F. Barbosa, J. Bettini, P.O. Luccas, E.C. Figueiredo, Direct extraction of lead (II) from untreated human blood serum using restricted access carbon nanotubes and its determination by atomic absorption spectrometry, *Talanta* 147 (2016) 478–484.
- K. Lou, Z.H. Zhu, H.M. Zhang, Y.Q. Wang, X.J. Wang, J. Cao, Comprehensive studies on the nature of interaction between carboxylated multi-walled carbon nanotubes and bovine serum albumin, *Chem. Biol. Interact.* 243 (2016) 54–61.
- T. Kopac, K. Bozgeyik, J. Yener, Effect of pH and temperature on the adsorption of bovine serum albumin onto titanium dioxide, *Colloids Surf. A Physicochem. Eng. Asp.* 322 (2008) 19–28.
- T. Kopac, K. Bozgeyik, Effect of surface area enhancement on the adsorption of bovine serum albumin onto titanium dioxide, *Colloids Surf. B: Biointerfaces* 76 (2010) 265–271.
- K. Bozgeyik, T. Kopac, Adsorption of bovine serum albumin onto metal oxides: adsorption equilibrium and kinetics onto alumina and zirconia, *Int. J. Chem. React. Eng.* 8 (A139) (2010) 1–26.
- T. Kopac, K. Bozgeyik, Equilibrium, kinetics and thermodynamics of bovine serum albumin adsorption on single-walled carbon nanotubes, *Chem. Eng. Commun.* 203 (9) (2016) 1198–1206.
- K. Bozgeyik, T. Kopac, Adsorption properties of arc produced multi walled carbon nanotubes for bovine serum albumin, *Int. J. Chem. React. Eng.* 14 (2) (2016) 549–558.
- O.H. Lowry, N.L. Rosebrough, A.L. Farr, R.J. Randall, Protein measurement with the folin phenol reagent, *J. Biol. Chem.* 193 (1951) 265–273.
- P. Puech, A. Bassil, J. Gonzalez, Ch. Power, E. Flahaut, S. Barrau, Ph. Demont, C. Lacabanne, E. Perez, W.S. Bacsa, Similarities in the Raman RBM and D bands in double-wall carbon nanotubes, *Phys. Rev. B* 72 (2005) 155436, <https://doi.org/10.1103/PhysRevB.72.155436>.
- S.J. Gregg, K.S.W. Sing, *Adsorption, Surface Area and Porosity*, second ed. Academic Press, London, 1982.
- K.S.W. Sing, R.T. Williams, Physisorption hysteresis loops and the characterization of nanoporous materials, *Adsorpt. Sci. Technol.* 22 (2004) 773–782.
- Y. Su-Dong, T. Xiu-Xiang, S. Kai-yi, Bio-solubilization of Chinese Lignite II: protein adsorption onto the lignite surface, *Min. Sci. Technol.* 19 (2009) 0363–0368.
- R. Duro, J.L. Gomez-Amoa, R. Martinez-Pacheco, C. Souto, A. Concheiro, Adsorption of polysorbate-80 on pyranol pamoate - effects on suspension stability, *Int. J. Pharm.* 165 (1998) 211–216.
- S.Y. Liu, J. Gao, Y.J. Yang, Y.C. Yang, Z.X. Ye, Adsorption intrinsic kinetics and isotherms of lead ions on steel slag, *J. Hazard. Mater.* 173 (2010) 558–562.
- S. Liang, X. Guo, N. Feng, Q. Tian, Isotherms kinetics and thermodynamic studies of adsorption of Cu²⁺ from aqueous solutions by Mg²⁺/K⁺ type orange peel adsorbents, *J. Hazard. Mater.* 174 (2010) 756–762.
- S.K. Behera, J.H. Kim, X. Guo, H.S. Park, Adsorption equilibrium and kinetics of polyvinyl alcohol from aqueous solution on powdered activated carbon, *J. Hazard. Mater.* 153 (2008) 1207–1214.

- [44] N. Gupta, S.S. Amritphale, N. Chandra, Removal of Zn (II) from aqueous solution by using hybrid precursor of silicon and carbon, *Bioresour. Technol.* 101 (2010) 3355–3362.
- [45] M. Monier, D.M. Ayad, D.A. Abdel-Latif, Adsorption of Cu (II), Cd (II) and Ni (II) ions by cross-linked magnetic chitosan-2-aminopyridine glyoxal Schiff's base, *Colloids Surf. B: Biointerfaces* 94 (2012) 250–258.
- [46] Y. Bulut, H. Aydın, Kinetics and thermodynamics study of methylene blue adsorption on wheat shells, *Desalination* 194 (2006) 259–267.
- [47] S.D. Faust, O.M. Aly, *Adsorption Processes for Water Treatment*, Butterworth Scientific Ltd., Boston USA, 1987.